

## A STUDY OF LITHIUM DEUTERIDE AS A MATERIAL FOR A POLARIZED TARGET

### Abstract

Experiment E155 at the Stanford Linear Accelerator Center (SLAC) measured the spin dependent structure of the proton and neutron, using for the first time  ${}^6\text{LiD}$  as the polarized deuteron target material in a high energy electron beam. This compound provides a significantly higher dilution factor than any other solid deuteron target material currently used in high energy physics experiments. Results of the polarization behavior of the  ${}^6\text{LiD}$  target material before and after exposure to the 50 GeV/ $c$  electron beam used in E155 are presented.

Keywords: Polarized Target; Lithium Deuteride; Spin; Structure Functions

PACS: 29.25.Pj

S. Bültmann<sup>1,\*</sup>, D. G. Crabb<sup>1,\*</sup>, D. B. Day<sup>1</sup>, R. D. Fatemi<sup>1</sup>, B. Gardner<sup>1,a</sup>,  
C. M. Harris<sup>1</sup>, J. R. Johnson<sup>2</sup>, J. S. McCarthy<sup>1</sup>, P. M. McKee<sup>1</sup>, W. Meyer<sup>3,b</sup>,  
S. I. Penttilä<sup>4</sup>, E. Ponikvar<sup>1,c</sup>, A. Rijllart<sup>5</sup>, O. A. Rondon<sup>1</sup>, S. St. Lorant<sup>3</sup>,  
W. A. Tobias<sup>1</sup>, S. Trentalange<sup>6</sup>, H. Zhu<sup>1</sup>, B. Zihlmann<sup>1</sup>, D. Zimmermann<sup>1,d</sup>

---

<sup>1)</sup> University of Virginia, Department of Physics, Charlottesville, VA 22901, USA

<sup>2)</sup> University of Wisconsin, Department of Physics, Madison, WI 53706, USA

<sup>3)</sup> Stanford Linear Accelerator Center, Stanford, CA 94309, USA

<sup>4)</sup> Los Alamos National Laboratory, Los Alamos, NM 87545, USA

<sup>5)</sup> CERN, CH-1211 Geneva 23, Switzerland

<sup>6)</sup> University of California, Department of Physics, Los Angeles, CA 90024, USA

<sup>a)</sup> Now at: Defense Group, Inc., Arlington, VA, USA

<sup>b)</sup> Permanent Address: Ruhr-Universität Bochum, Fakultät für Physik, D-44780 Bochum, Germany

<sup>c)</sup> Now at: Electronic Data Systems, Alexandria, VA, USA

<sup>d)</sup> Now at: Informix Software, Inc., Portland, OR 97205, USA

<sup>\*</sup>) Corresponding authors

E-mail: bueltman@cebaf.gov, dgc3q@virginia.edu

## Introduction

Knowledge of the internal spin structure of the nucleon is accessible through deep-inelastic scattering of polarized leptons off polarized nucleon targets. Often chosen are polarized solid targets, offering a large number of polarized nucleons per square centimeter [1, 2, 3]. To measure the proton spin structure, target materials with a high hydrogen content, such as solid butanol and solid ammonia, are typically used. As targets with free neutrons are not available, the neutron spin structure has to be measured indirectly. One approach is to compare the spin dependent scattering off polarized proton and deuteron targets. Therefore, butanol and ammonia in their deuterated forms are often employed [4].

The free nucleons in the solid target material are polarized by the Dynamic Nuclear Polarization (DNP) technique, which requires a low temperature, a high magnetic field, and an oscillating magnetic field in the microwave range. The nuclear polarization is usually measured by Nuclear Magnetic Resonance (NMR).

An earlier experiment, E143, at the Stanford Linear Accelerator Center (SLAC) used the polarized electron beam and polarized ammonia targets [5]. In preparation for the new experiment E155,  $^6\text{LiD}$  was tested as a possible candidate for the deuteron target. Encouraging results from a nuclear physics experiment, using proton and neutron beams, were reported in Ref. [6]. The results obtained with different samples, prior to and during the experiment, are presented in this paper and compared to earlier results and to those obtained with other target materials.

The polarized target used for these measurements is similar to the target used in E143 and is described in Ref. [5]. It features a 5 T superconducting magnet, a  $^4\text{He}$  evaporation refrigerator operating at about 1 K, and an Extended Interaction Oscillator (EIO) generating microwaves at 140 GHz. The polarization in the cylindrical cavity is measured by a NMR system using Liverpool  $Q$ -meters [7].

## Comparison of Different Polarized Target Materials

A suitable material for a polarized solid target has to fulfill several criteria. Among them are a high dilution factor,  $f$ , giving the fraction of polarizable nucleons, high polarization, fast polarization build up, and radiation hardness. The latter is of particular importance in the case of a high intensity charged particle beam. The materials of choice for polarized solid proton targets today are alcohols, such as butanol, and ammonia, while the hydrogen atoms are replaced by deuterons in case of polarized deuteron targets. The paramagnetic centers necessary for DNP are introduced in the target material by chemical or radiation doping. Radicals, such as EHBA–Cr(V), are added by chemical doping in the case of butanol [8]. At room temperature, these EHBA crystals are easily soluble in the butanol, which then can be frozen into small glassy beads. In the case of ammonia, the frozen material is irradiated in a charged particle beam at a temperature around 90 K [5]. Adding dopants to gaseous or solid materials is difficult and, for example, led to limited success in ammonia. To ensure uniform cooling during DNP, the target material is commonly prepared in the form of small granules or beads of roughly equal size. This

will help in ensuring a homogeneous polarization throughout the target. To obtain small pieces, the liquid or gaseous raw material is either frozen into a block and afterwards crushed into small pieces or dripped onto the surface of a liquid nitrogen bath to obtain beads.

Results of a promising new deuteron target material were published by Abragam and co-workers in 1980 [9, 10]. Lithium deuteride,  ${}^6\text{LiD}$ , has a favorable dilution factor in comparison to the materials mentioned above, if the  ${}^6\text{Li}$  nucleus is regarded as a polarizable neutron-proton pair plus a spectator alpha particle. This simple nuclear structure model is supported by the magnetic moments of the spin-1 nuclei, which are  $\mu_2 = 0.857 \cdot \mu_N$  and  $\mu_6 = 0.822 \cdot \mu_N$ , where  $\mu_N$  is the nuclear magneton. Details about this assumption will be discussed in the following section.

The measurements of Abragam and co-workers were carried out at different magnetic fields and in a dilution refrigerator operating below 200 mK during DNP. It was found that with increasing magnetic field, the maximum polarizations for deuterons and  ${}^6\text{Li}$  nuclei increased. At 6.5 Tesla a maximum  ${}^6\text{Li}$  polarization of  $P_6 = 0.71$  was reached, while at 2.5 Tesla  $P_6 = 0.40$  was obtained. For E155, with its high intensity electron beam, a  ${}^4\text{He}$  evaporation refrigerator with its high cooling power is needed, which leads to an expectation for a lower maximum polarization around  $P_6 = 0.20$ .

Most deuteron target materials have a broad, double peaked, NMR signal due to overlapping transitions, because of the interaction of the deuteron electric quadrupole moment with the electric field gradient of the lattice [11]. These field gradients are missing in the face-centered cubic (fcc) structure of the lithium deuteride crystal lattice. The resulting NMR signals of the deuteron and lithium are therefore very narrow and easy to measure with a FWHM of about 6 G.

The dilution factors and typical polarization values for the different deuteron targets are given in Table 1. This dilution factor is an approximation, neglecting the EMC-effect and other kinematic dependent corrections. The deuteron polarization of  ${}^6\text{LiD}$  is slightly larger than the lithium polarization due to the larger magnetic moment of the deuteron. The values for the deuteron polarization were not reported in Ref. [10].

The  ${}^6\text{LiD}$  material used for this experiment is a sinter with the physical properties of a hard sandstone which allows the preparation of small pieces at room temperature. By crushing the sintered material and sieving the resulting smaller pieces, chips of two sizes, 1.0 mm to 2.5 mm, and, 2.5 mm to 3.5 mm, later referred to as small and large chips, were obtained. The chips have to be kept in a dry gas atmosphere, here dry nitrogen gas, to prevent the disintegration into lithium hydroxide.

An isotopic analysis of the target material revealed that 4.6% (molar) of the lithium is  ${}^7\text{Li}$ , having a spin of  $I = \frac{3}{2}$  and a magnetic moment of  $3.256 \cdot \mu_N$ . The material was also found to be not fully deuterated with a molar percentage of 2.4 being hydrogen. As these isotopic impurities are polarizable, they do contribute to the spin dependent scattering cross section and have to be taken into account by measuring their respective polarizations.

## Spin Structure of Nuclei

The use of  ${}^6\text{LiD}$  as a polarized target in spin structure experiments requires that proper allowance be made for the nuclear properties of both lithium and deuterium. This involves both an understanding of the magnitude of the contributions of the polarized nucleons in each nuclear species to the spin asymmetries, as well as the possible kinematic ( $x_{\text{BJ}}$ ) dependence of the nucleon polarization.

Two approaches are commonly considered. In the case of isospin singlets, like  ${}^2\text{H}$ ,  ${}^6\text{Li}$ , and  ${}^{14}\text{N}$ , model independent analyses using only isospin conservation can be applied, based on the decomposition of the total nuclear angular momentum,  $I$ , and magnetic moment,  $\mu$ , in terms of spin and orbital components [14]. In the case of mirror nuclei, like  ${}^3\text{H}$  and  ${}^3\text{He}$ , or  ${}^{15}\text{N}$  and  ${}^{15}\text{O}$ , this analysis can be supplemented by information from the beta decay of one of the pair members [15, 16]. The cluster model description of light nuclei, such as lithium [17], allows the extension of this method to the cluster components of  ${}^7\text{Li}$ .

The second approach involves shell models of the nuclear structure. This approach has been used to describe the nucleon polarization of  ${}^2\text{H}$  [18],  ${}^3\text{He}$  [19],  ${}^6\text{Li}$  [18, 20],  ${}^{14}\text{N}$  [21, 22], and  ${}^{15}\text{N}$  [3]. At the simplest level, the relevant information to be extracted from the models consists of the probabilities of the different nuclear states and their corresponding angular momentum decompositions. This information allows a proportionality factor between the nucleon and the nucleus polarizations to be calculated.

Using the first approach, the values of the nucleon polarization in  ${}^2\text{H}$  and  ${}^6\text{Li}$  are estimated to be 94% and 85% of the nuclear polarization, respectively. These values are in excellent agreement with those obtained from nuclear structure models. For the deuteron, the nucleons in the  $D$ -state have their spins aligned opposite to the nuclear spin a net 50% of the time, while the nucleons in the  $S$ -state are always aligned along the nuclear spin. Combining this with a 5% occupation probability of the  $D$ -state [23], the nucleon polarization in  ${}^2\text{H}$  is 92.5% of the deuteron polarization.

With  ${}^6\text{Li}$ , the situation is somewhat more complex. A three-body cluster model of  ${}^6\text{Li}$  [20] ( $\alpha + p + n$ ) indicates that  $P$ - and  $P'$ -states are also present, in agreement with the predictions of the model-independent approach [14], neglecting small isospin breaking effects. While in Ref. [20] definite values for each of the states' probabilities are given, the nucleon spin components are incorrectly assigned. Using the correct spin assignments, one obtains for the nucleon spin

$$P_n = 1 - \frac{1}{2}P - P' - \frac{3}{2}D, \quad (1)$$

where  $P$ ,  $P'$ , and  $D$  represent the probabilities of each orbital angular momentum state. Taking from [20] the average of seven models with adequate predictions for properties of  ${}^6\text{Li}$ , such as the magnetic moment, charge radius, and charge form factor, one obtains  $P_n = 0.866 \pm 0.012$ , which is in good agreement with the model independent prediction.

The presence of  ${}^7\text{Li}$  in the LiD used in this experiment requires that the contributions of this nucleus to the asymmetry be understood. While the model independent analysis is valid for  ${}^7\text{Li}$ , there is no measurement of the magnetic moment of its very short lived

mirror pair  ${}^7\text{Be}$  that could be used for this purpose.  ${}^7\text{Li}$  is very well described as an  $\alpha$ -triton pair of clusters [17]. This feature allows the nucleon polarization in  ${}^7\text{Li}$  to be described in terms of the corresponding nucleon polarization in tritium. Following the model independent approach, the polarization of the proton in  ${}^3\text{H}$  is 94% of the tritium polarization. The tritium and alpha clusters form an  $I = \frac{3}{2}$  system where the spin of the tritium cluster is aligned parallel to the lithium spin  $2/3$  of the time. Thus the net proton spin polarization in  ${}^7\text{Li}$  is  $(62.7 \pm 1.4)\%$ .

It has been shown recently [24], that in the kinematic range  $x_{\text{Bj}} < 0.75$ , the use of a constant factor to correct for the presence of  $D$ -state nucleons in the deuteron results in a deviation of less than 1.5% from the more accurate convolution or covariant descriptions. Since the uncertainty in the  $D$ -state probability itself is on the order of  $\simeq 1\%$  (20% relative), the use of a constant correction factor, at least in the measured kinematic range ( $0.015 < x_{\text{Bj}} < 0.75$ ), is valid in the case of the deuteron. For the extraction of the neutron spin structure, more refined descriptions of the nucleon polarization may be necessary, given the small size of the deuteron asymmetry at low  $x_{\text{Bj}}$ . The level of required refinement becomes more important with increasing nuclear complexity, as in the cases of  ${}^3\text{He}$  and  $\text{Li}$ .

### Irradiation of ${}^6\text{LiD}$ Material

The irradiation of the target material was carried out at the 30 MeV electron Linac of the SUNSHINE<sup>1)</sup> facility at Stanford University. The  ${}^6\text{LiD}$  was subjected to a range of electron fluxes from  $1.3 \cdot 10^{17} \text{ e}^-/\text{cm}^2$  to  $4.5 \cdot 10^{17} \text{ e}^-/\text{cm}^2$ . For simplicity, during the course of this paper, we will refer to this quantity as dose. The cross section of the cylindrical target material container was 20 mm in diameter. In order to irradiate the  ${}^6\text{LiD}$  homogeneously, the width of the approximately Gaussian shaped beam was widened to about 25 mm, which resulted in an effective fraction of the beam hitting the target of 25%. With an average current of  $2.5 \cdot 10^{12} \text{ e}^-/\text{spill}$  and a rate of 20 Hz, the target material had to be irradiated for two hours to achieve a total of  $1.0 \cdot 10^{17}$  electrons. Extensive investigations of the irradiation temperature leading to the highest deuteron polarization were carried out predominantly at Saclay [25, 26] and Bonn [27]. It was found that the temperature of the lattice governs the rate of recombination of the color centers created by the electron beam. The preferred temperature was determined to be  $183 \text{ K} \pm 3 \text{ K}$ , which requires a more involved irradiation cryostat than used for the ammonia irradiations. For this purpose a dewar with circulating helium gas being cooled by liquid nitrogen was built, as shown in Fig. 1.

The target material was contained in a stainless steel mesh cylinder being 20 mm in diameter and 50 mm in length, giving a volume of  $16 \text{ cm}^3$ . The helium gas entering at the top of the irradiation dewar was cooled down while passing the liquid nitrogen shield. Reaching the bottom of the dewar it streamed up towards the target material and warmed by heater wire to the desired temperature. The power of the heater wire was adjusted according to the gas temperature as measured with a platinum resistor just above the

---

<sup>1)</sup> Stanford UNiversity SHort INTense Electron source

target material. The temperature of the target material was also adjustable by changing the pumping speed of the gas circulating compressor. A temperature of 183 K could be maintained within 3 K.

### Polarized Target System

The irradiated target material was polarized in the polarized target setup, which was later used in E155. A superconducting split coil magnet<sup>2)</sup> generated a 5 T field with a homogeneity of  $10^{-4}$  over a sphere of 30 mm diameter. The target material was contained in cylinders of 27 mm in diameter and 30 mm in length. Polarization measurements prior to E155 were carried with inserts featuring one target container made out of Torlon. Later during E155, two metal containers were arranged, one on top of the other, in an insert, which could be moved vertically to place either container in the homogeneous field region. The inserts could be changed, without warming up the refrigerator, within 15 minutes. The target material was cooled by a  $^4\text{He}$  evaporation refrigerator having a cooling power of about 1 W at 1 K. A base temperature of about 0.95 K was reached. With the added heat load of about 1.1 W from microwaves and the electron beam, a temperature of 1.07 K could be maintained. To prevent excessive and non-uniform beam heating of the target volume, the beam was rastered over the target face of  $5.7\text{ cm}^2$  with a raster pattern radius of 10 mm. The beam size was about 3 mm with a space of 0.3 mm between individual raster points. The temperature of the liquid  $^4\text{He}$  was measured primarily by the vapor pressure of liquid  $^3\text{He}$  contained in a sealed, small diameter tube and connected to a capacitive pressure gauge. In addition the  $^4\text{He}$  vapor pressure inside the refrigerator was measured with another capacitive pressure gauge. Carbon glass and ruthenium oxide resistance thermometers were used as secondary standards.

The electron Larmor frequency in a 5 T field is in the microwave range around 140 GHz. An Extended Interaction Oscillator (EIO)<sup>3)</sup>, with 20 W of source power, generated the microwaves, which were guided over a total length of 2 m to the target cell. The microwave power at the cell was less than 1 W. To ensure maximum and equal microwave power at each target container for the two container inserts, the target material was contained in copper coated aluminum cylinders, acting as cavities, and fed by individual wave guides inside the insert. The microwaves were switched to either waveguide on the outside of the target.

### Polarization Measurement

Polarization of the different nuclei present in the  $^6\text{LiD}$  target material was measured by NMR, using commercially available series tuned  $Q$ -meters [7]. The  $Q$ -meters were connected to NMR coils, which were embedded in the target material, forming a tuned series  $LRC$ -circuit. With changing polarization of the nucleons, the nuclear magnetic susceptibility changes, which in turn changes the inductance of the coil. This leads to a measurable voltage change in the  $LRC$ -circuit, provided a constant current is supplied to

---

<sup>2)</sup> Oxford Instruments, Scientific Research Division, England

<sup>3)</sup> CPI, Canada

the circuit. By sweeping the NMR through the nuclear Larmor frequency a spin resonance signal is obtained. The strength of the signal, that is the integrated resonance signal over the sweep range, is linearly proportional to the polarization of the nuclei.

Each target cavity was equipped with two NMR coils of different inductance for the measurement of the different nuclear polarizations. A horizontal straight wire or wire loop of one turn, giving a small inductance of about 30 nH, was used for the protons and  $^7\text{Li}$  nuclei. For the deuterons and  $^6\text{Li}$  nuclei a loop with 4 turns across the target cross section with an inductance of about 180 nH was used. The coils were made out of CuNi (70/30) tubing with an outer diameter of 0.5 mm. The coils were connected to the  $Q$ -meters via coaxial cables of two half integer wave lengths, thereby minimizing the cable attenuation of the resonance signals.

By measuring the nuclear spin resonance signal and its integral,  $\Gamma_{\text{TE}}$ , at a given magnetic field and a known temperature, and by calculating the polarization,  $P_{\text{TE}}$ , under these conditions, the resonance circuit was calibrated. The integral over a resonance signal after polarization enhancement,  $\Gamma$ , results in a polarization of  $P = \Gamma \cdot P_{\text{TE}} / \Gamma_{\text{TE}}$ . The time to reach this thermal equilibrium (TE) is reduced with increasing temperature. Most calibrations were carried out at about 1.5 K to 1.8 K, still well below the  $\lambda$ -point of  $^4\text{He}$ . Several fast calibrations were done at a higher temperature around 3.3 K, but it was more challenging to stabilize the temperature and to establish TE under these conditions. The time to reach thermal equilibrium varied from about five hours at around 3.3 K to about twelve hours at 1.8 K. A representative deuteron TE signal taken at 3.3 K is shown in Fig. 2. The natural deuteron polarization at 5 Tesla and 3.3 Kelvin is  $P_{2(\text{TE})} = +0.0003$ . In contrast to most other deuteron target materials the deuteron signal in  $^6\text{LiD}$  is very narrow with a FWHM of 4 kHz. A negatively enhanced deuteron signal of  $P_2 = -0.22$  polarization is shown in Fig. 3.

## Results after pre-irradiation

In this section we present data obtained before using the  $^6\text{LiD}$  target material in the SLAC electron beam. The main purpose of the pre-E155 studies was to find the optimal pre-irradiation dose and to establish that the deuteron and  $^6\text{Li}$  nuclear polarizations follow the prediction of an Equal Spin Temperature (EST). In the spin temperature concept the energy states of a spin species are described by a Boltzmann distribution with a characteristic spin temperature. In the framework of EST it is assumed that each spin species in a target material has the same spin temperature while driving the electron Larmor frequency. Then the polarization of each spin species depends only on the magnetic moment of that species. Establishing the validity of EST for a given target material therefore allows the monitoring of the polarization of only one spin species and calculating the other polarizations from this measurement.

In Fig. 4 the polarizations of the  $^6\text{Li}$  and  $^7\text{Li}$  nuclei in lithium deuteride are shown as a function of the deuteron polarization. These three spin species were measured sequentially. The lithium polarizations calculated from the deuteron polarizations assuming EST are shown as full lines in the plot. A very good agreement between EST prediction

and the measured lithium polarizations can be seen. This is in agreement with observation of others [27].

A suitable pre-irradiation dose should lead to high deuteron and  ${}^6\text{Li}$  polarizations, to a short polarization build-up time, and rapid attainment of thermal equilibrium for calibration of the polarization. In Fig. 5 the maximum deuteron polarization for different pre-irradiation doses is shown. As expected, a favorable region around  $3.0 \cdot 10^{17} \text{ e}^-/\text{cm}^2$  was found. For an optimum dose, the different counteracting processes involved in the polarization build-up have to be balanced. A low pre-irradiation dose leads to an insufficient amount of paramagnetic centers per nucleon spin and the polarization of the whole target is limited by the slow spin diffusion process. In case of a too high pre-irradiation dose, the relaxation mechanisms between nucleon and electron spins become dominant, therefore counteracting the polarization build-up.

This can be seen in Fig. 6 showing the deuteron polarization build-up of four samples with different pre-irradiation doses. The sample with the lowest pre-irradiation dose polarizes slowly compared to the other samples. The sample with initially the fastest build-up has the highest dose but does not reach a very high polarization.

The polarization behavior as a function of the polarizing microwave frequency was also measured prior to E155. For these measurements, the target was initially at a low polarization of about  $P = 0.1$ . As the magnetic field has to be kept constant, because of the tuned NMR circuit, the microwaves were slowly stepped through a frequency range comprising the two frequencies leading to positive and negative polarization enhancement. The shape of the resulting curve and the position of the two peaks for the optimum frequencies depends on the  $g$ -factor of the electrons. A representative plot for a dose of  $2.0 \cdot 10^{17} \text{ e}^-/\text{cm}^2$  is shown in Fig. 7. The distance between the two optimum polarizing frequencies is about 50 MHz or 18 G, a value reported also in Ref. [27]. If DNP would be dominated by the solid effect mechanism [28], a frequency of twice the deuteron Larmor frequency, 65 MHz, would be expected.

In Fig. 8 the relaxation times,  $\tau$ , for four target samples, each with different pre-irradiation doses, are shown as a function of the inverse temperature. If the relaxation is dominated by a single type of paramagnetic center the relation

$$\tau = \exp\left(\frac{g \mu_B B}{2 k T}\right)$$

describes the relaxation time in the limit  $\mu_B B \gg k T$ . Here  $g$  is the Landé  $g$ -factor,  $\mu_B$  the Bohr magneton,  $B$  the magnetic field,  $k$  the Boltzmann constant, and  $T$  the temperature. A fit to the measurements, indicated by the solid line in Fig. 8, results in a  $g$ -factor of  $2.15 \pm 0.17$ . For comparison, the slope of the dashed line in Fig. 8 corresponds to a  $g$ -factor of 2. The deviation is very small. Results obtained earlier in Bonn [27] and Saclay [10] show a larger deviation with a  $g$ -factor of about 3 in the same temperature range. This indicates the presence of a second paramagnetic center with a larger  $g$ -factor or a non-electronic relaxation channel. The Saclay measurements over their entire temperature range, however, agree with our measurement of a  $g$ -factor of about 2.



## Effect of High Energy Electron Beam Exposure

Prior to E155, not much was known about the behavior of  ${}^6\text{LiD}$  in a high intensity and high energy electron beam. Based on our knowledge at the time, an initial target material with a pre-irradiation dose of  $3.7 \cdot 10^{17} \text{ e}^-/\text{cm}^2$  was chosen (see Fig. 5). It was then exposed at a temperature slightly above 1 K to the 50 GeV/ $c$  electron beam with an average current of about 80 nA. In Fig. 9, deuteron polarization build-up curves of this material with three accumulated doses are shown. A small dose leads to faster polarization build-up, compared to the pre-irradiation. This is in agreement with earlier observations [27] and also agrees with measurements made with deuterated ammonia [5]. With increasing dose, however, the build-up times get longer and the achievable polarization lower.

During E155 a maximum deuteron polarization of  $P_2 = -0.32 \pm 0.01$  and a  ${}^6\text{Li}$  polarization of  $P_6 = -0.31 \pm 0.01$  was achieved. The  ${}^6\text{Li}$  polarization was regularly monitored and followed the deuteron polarization as expected from EST. E143 used deuterated ammonia and reached  $P_2 = +0.40$  [5], but deuterated ammonia features a lower dilution factor than  ${}^6\text{LiD}$  when taking the  ${}^6\text{Li}$  polarization into account.

A full deuteron polarization history is shown in Fig. 10 for target material with a pre-irradiation dose  $2.0 \cdot 10^{17} \text{ e}^-/\text{cm}^2$ . It can be seen, that the polarization increases with the accumulated dose until it reaches a maximum at about  $5.0 \cdot 10^{15} \text{ e}^-/\text{cm}^2$ . The structure in the curves results from interruptions of the beam and normalizing measurements with unpolarized targets. These led to partial losses of polarization and therefore the need to rebuild the polarization. With increasing dose, the time for these re-polarizations increases, consistent with the observations made with the  $3.7 \cdot 10^{17} \text{ e}^-/\text{cm}^2$  sample. A comparison of lithium deuteride and deuterated ammonia shows the same overall polarization behavior as a function of the radiation dose. The main difference is the better radiation resistance of  ${}^6\text{LiD}$  with its maximum polarization radiation dose five times higher than that for ammonia.

When the dose of a sample reached about  $10^{16} \text{ e}^-/\text{cm}^2$  the material was annealed. This procedure was found to work very well in ammonia targets and was used frequently during E143 [5]. During an annealing process the lithium deuteride target was heated to about 185 K, the initial optimum pre-irradiation temperature. This was done by heater wire wrapped around the aluminum support structure of the target cell. The liquid helium boiled off and the target was kept backfilled with helium gas. The temperature was monitored inside the target cell by platinum resistors (Pt-100) and thermocouples. The temperature of about 185 K was maintained for 20 minutes before the heater was turned off and the target cooled down again. After the anneal, the same maximum polarization as previously was attained. However, the rate of polarization decay with increasing charge was faster than before the anneal. This observation was based on two anneals during E155 and is therefore statistically limited.

During E155 the optimal microwave frequency for enhancing the negative polarization was found to be 140.310 GHz. However, during irradiation with the 48 GeV electron beam, the optimal frequency consistently increased to 140.320 GHz.

## Conclusions

The polarization behavior of  ${}^6\text{LiD}$  as the polarized deuteron target in a scattering experiment using a high energy and high intensity electron beam was presented. In comparison with other polarized target materials, such as deuterated ammonia, lithium deuteride shows a superior radiation resistance, high polarizations and good polarizability, and an excellent dilution factor when taking the  ${}^6\text{Li}$  polarization into account. The major disadvantage of  ${}^6\text{LiD}$  is its long thermalization time, requiring extensive calibration.

## Acknowledgements

The authors wish to express their deep gratitude to D. Bocek, M. Hernandez, C. Settakorn, and H. Wiedemann of SUNSHINE at Stanford University for providing excellent irradiation conditions at their facility and many hours of help. The technical support of the SLAC EF Division with W. Kaminskas, W. Nichols, R. Pitthan, and M. Racine was indispensable. This work was supported in part by the Institute of Nuclear and Particle Physics at the University of Virginia and the US Department of Energy under Grant No. DE-FG02-96ER40950 and contract DE-AC03-76SF00515.

## References

- [1] B. Adeva et al., Phys. Lett. B **302**, 533 (1993).
- [2] D. Adams et al., Phys. Lett. B **329**, 399 (1994).
- [3] K. Abe et al., Phys. Rev. Lett. **74**, 346 (1995).
- [4] D. G. Crabb and W. Meyer, Annu. Rev. Nucl. Part. Sci. **47**, 67 (1997).
- [5] D. G. Crabb and D. B. Day, Nucl. Instr. and Meth. A **356**, 9 (1995).
- [6] J. Ball et al., Nucl. Instr. and Meth. A **381**, 4 (1996).
- [7] G. R. Court et al., Nucl. Instr. and Meth. A **324**, 433 (1993).
- [8] S. Bültmann et al., Nucl. Instr. and Meth. A **356**, 102 (1995).
- [9] A. Abragam et al., J. Physique **41**, 309 (1980).
- [10] V. Bouffard et al., J. Physique **41**, 1447 (1980).
- [11] W. De Boer, J. of Low Temp. Phys. **22**, 185 (1976).
- [12] B. Bolden et al., Part. and Fields **49**, 175 (1991).
- [13] D. Adams et al., Phys. Lett. B **396**, 338 (1997).
- [14] R. G. Sachs, Phys. Rev. **69**, 611 (1946).
- [15] K. Sugimoto, Phys. Rev. **182**, 1051 (1969).
- [16] B. A. Brown and B. H. Wildenthal, Phys. Rev. C **28**, 2397 (1983).
- [17] H. Walliser and T. Fliessbach, Phys. Rev. C **31**, 2242 (1985).
- [18] L. Frankfurt and M. I. Strikman, Nucl. Phys. **A405**, 557 (1983).
- [19] J. L. Friar et al., Phys. Rev. C **42**, 2310 (1990).
- [20] N. W. Schellingerhout et al., Phys. Rev. C **48**, 2714 (1993),  
*err.* Phys. Rev. C **52**, 439 (1995).
- [21] J. Ashman et al., Phys. Lett. B **206**, 364 (1988).
- [22] J. Ashman et al., Nucl. Phys. B **328**, 1 (1989).
- [23] K. Abe et al., Phys. Rev. Lett. **75**, 25 (1995).

- [24] W. Melnitchouk et al., Phys. Lett. B **346**, 165 (1995).
- [25] Y. Roinel et al., J. Physique **39**, 1097 (1978).
- [26] P. Chaumette et al., in *Proc. of the International Workshop on Polarized Sources and Targets*, Montana (Switzerland) 1986.
- [27] S. Goertz et al., Nucl. Instr. and Meth. A **356**, 20 (1995).
- [28] M. Borghini, in *Proc. of the IInd International Conference on Polarized Targets*, Berkeley (USA) 1971, 1 (1971).

Material	Dopant	$f$	$P_2$	$P_6$	$B/T$	$T/K$	Ref.
$^{14}\text{ND}_3$	Irradiation	0.30	0.49		2.5	0.20	[12]
$^{15}\text{ND}_3$	Irradiation	0.29	0.42		5.0	1.05	[5]
$\text{C}_4\text{D}_{10}\text{O}$	EDBA Cr(V)	0.24	0.50		2.5	0.30	[13]
$^6\text{LiD}$	Irradiation	0.50		0.71	6.5	0.25	[10]
				0.64	4.9	0.25	[10]
				0.40	2.5	0.25	[10]

Table 1: Naive dilution factor,  $f$ , and polarizations of  $^2\text{H}$  and  $^6\text{Li}$  obtained at different magnetic fields,  $B$ , and temperatures,  $T$ .

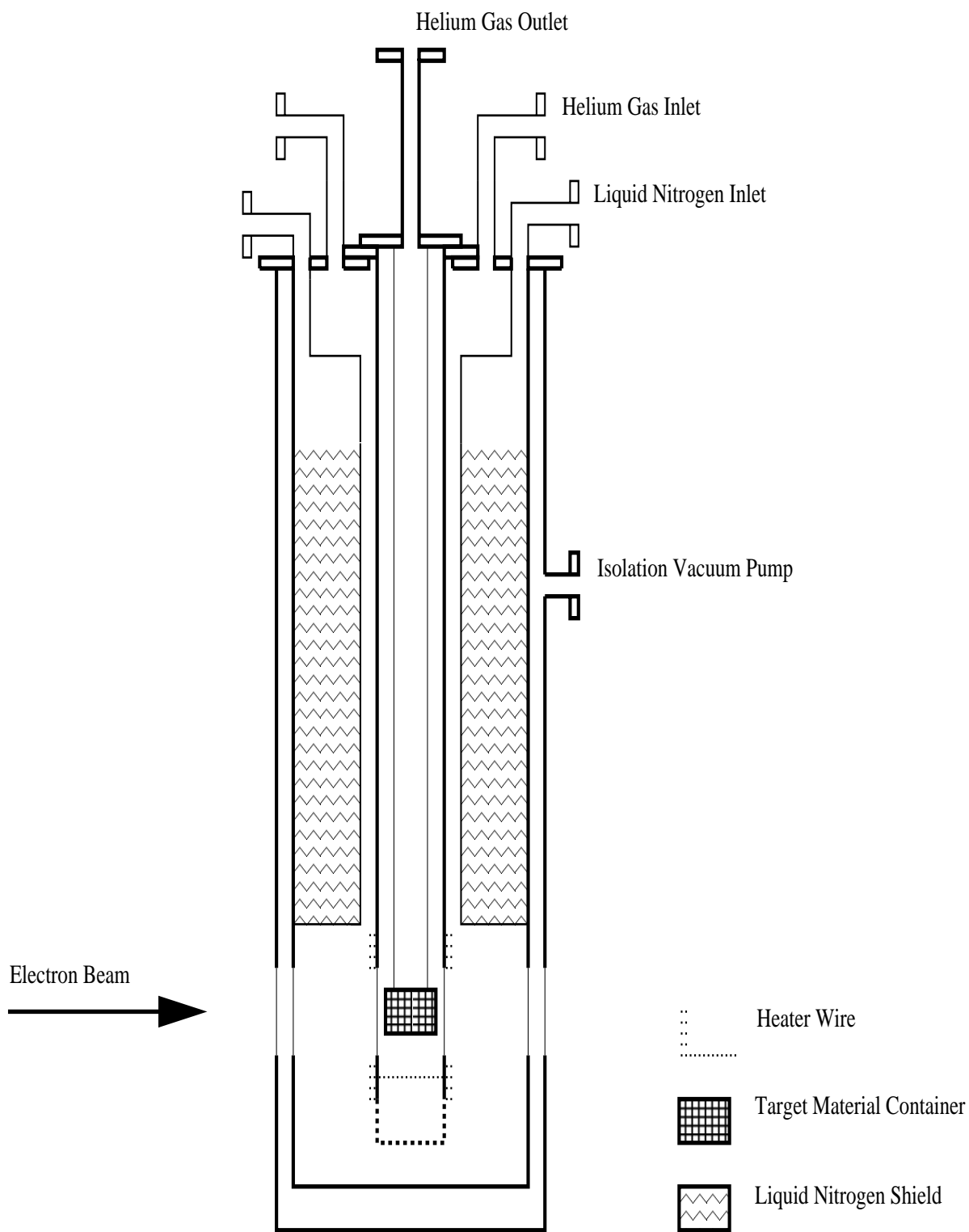


Figure 1: The irradiation dewar for the lithium deuteride target material. The material is cooled by circulating He gas at 183 K. The gas is cooled by a liquid nitrogen shield and temperature controlled by a heater.

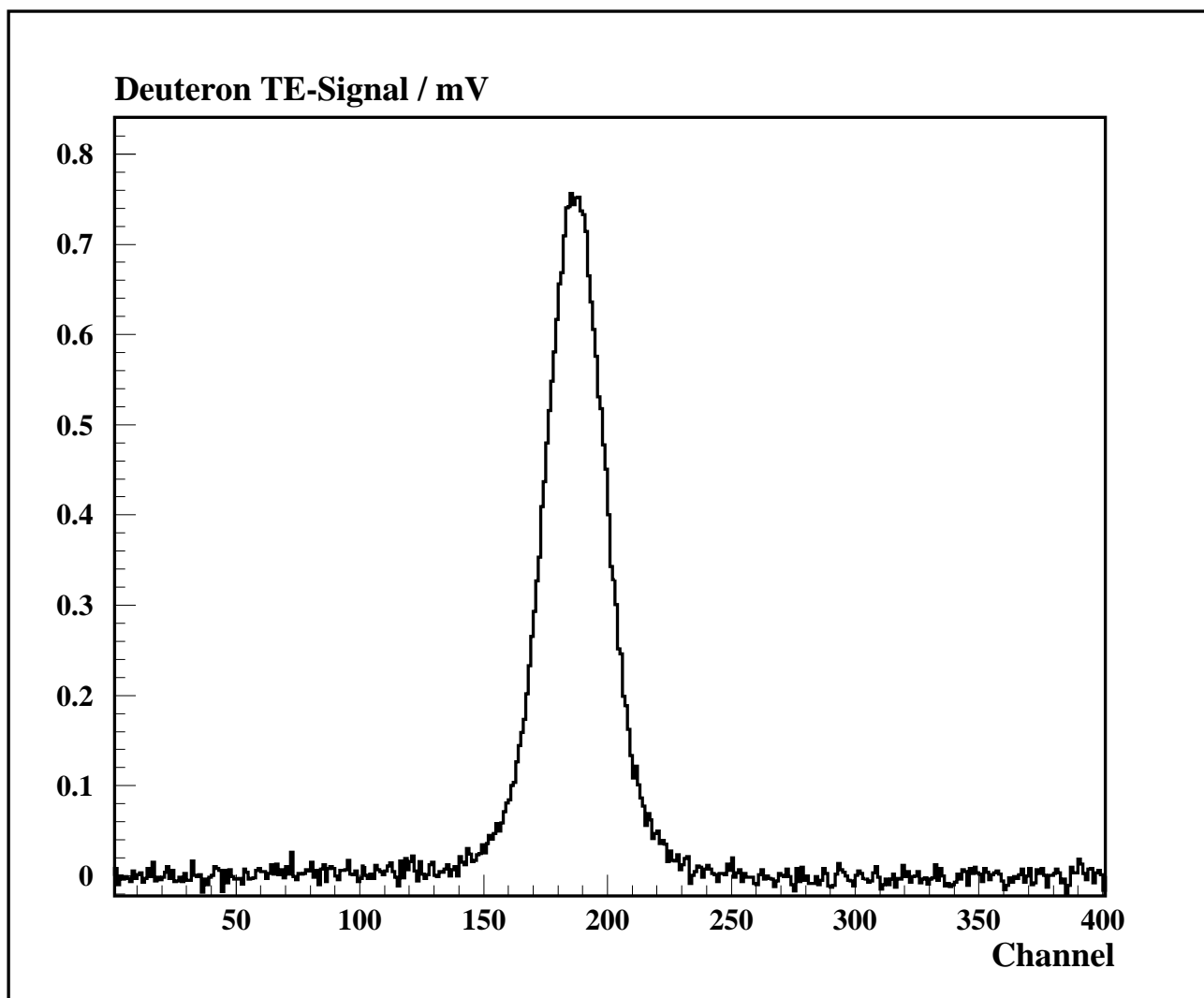


Figure 2: Deuteron thermal equilibrium (TE) NMR signal in  ${}^6\text{LiD}$  at 3.3 K, averaged from 1000 double sweeps. The 400 channel plot corresponds to a frequency range of 32.709 MHz  $\pm$  25 kHz.

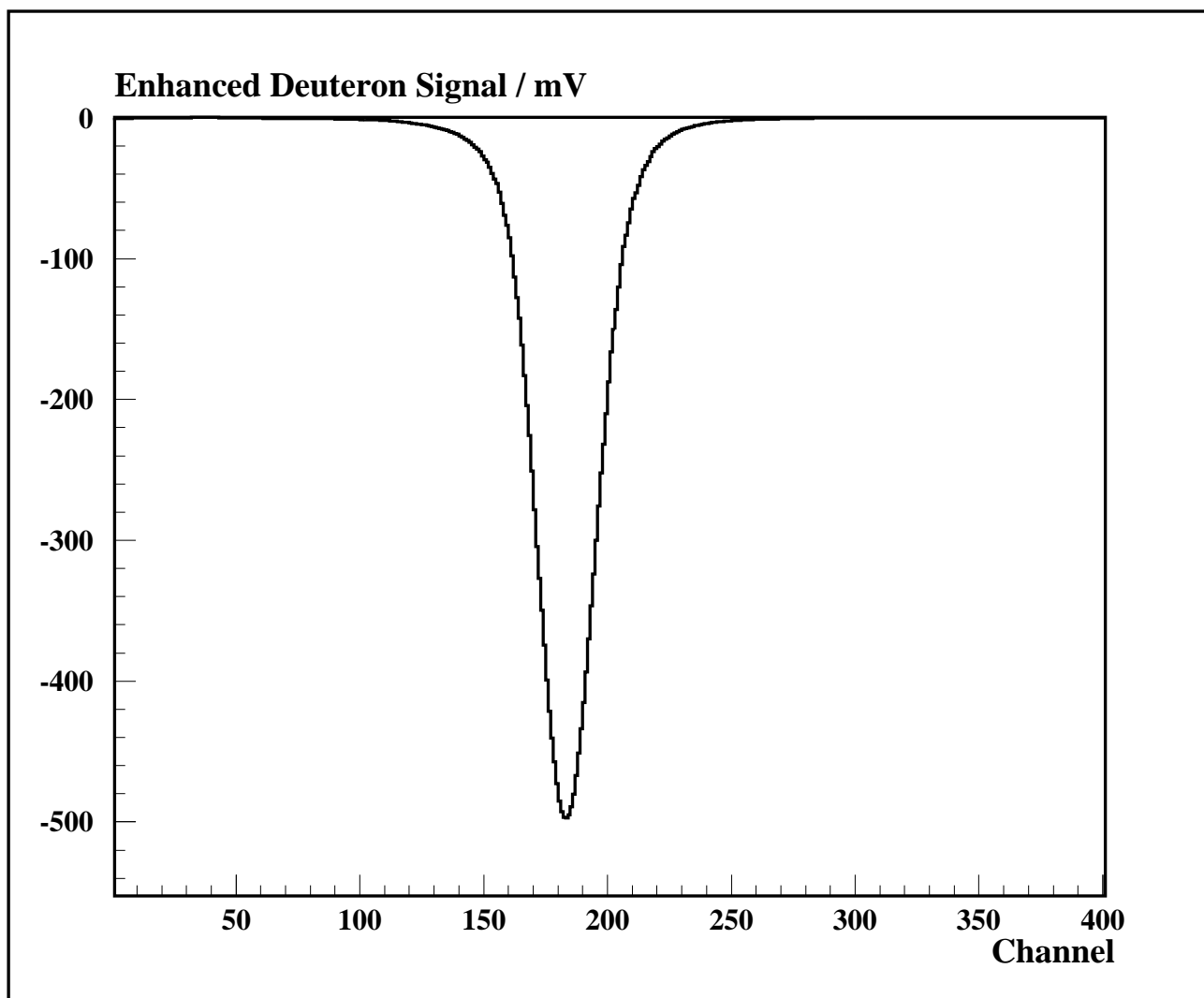


Figure 3: Enhanced deuteron NMR signal of  $-0.22$  polarization in  ${}^6\text{LiD}$ , taken with 200 double sweeps. The 400 channel plot corresponds to a frequency range of  $32.709\text{ MHz} \pm 25\text{ kHz}$ .

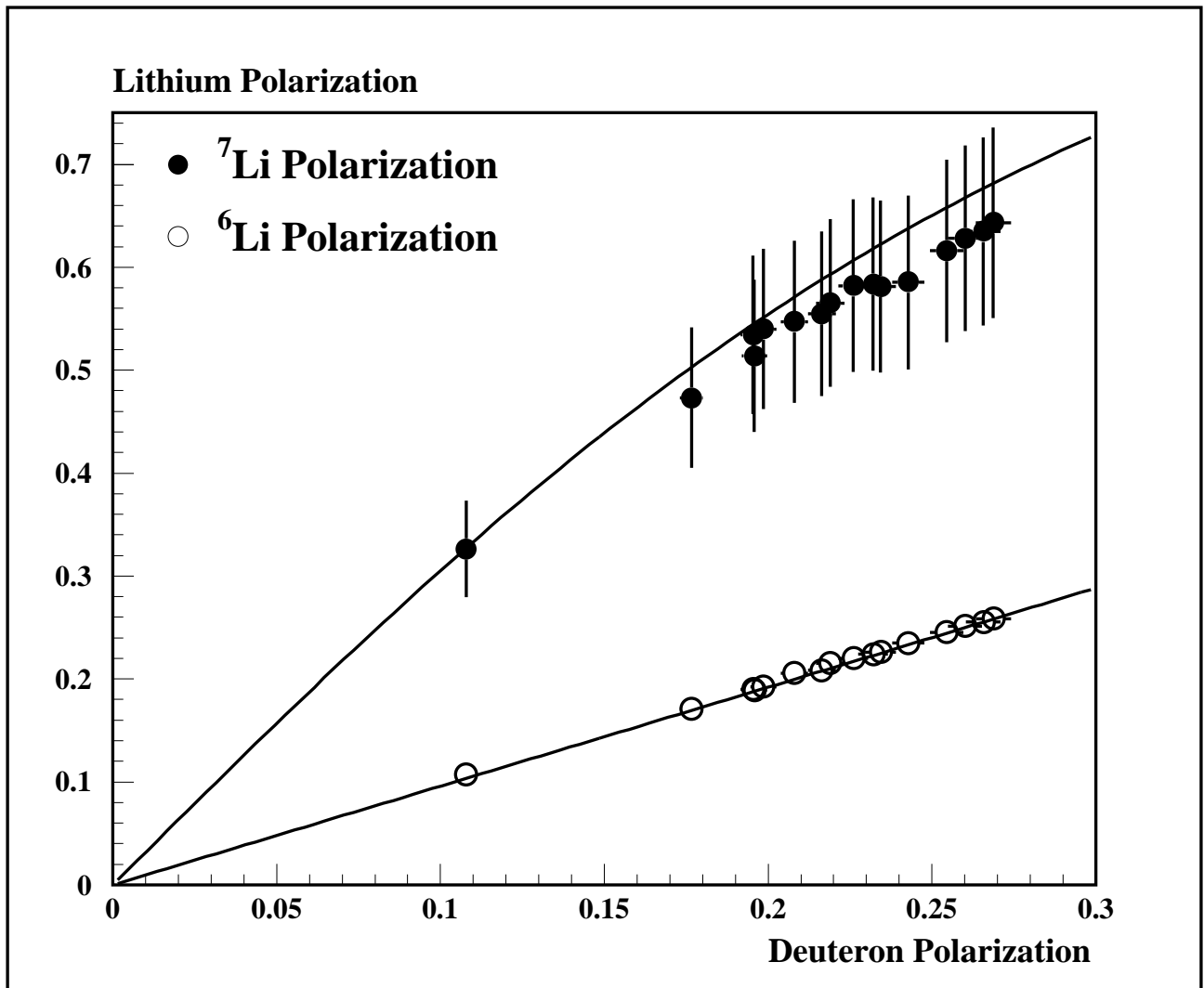


Figure 4: Measured polarization of  ${}^6\text{Li}$  and  ${}^7\text{Li}$  nuclei as a function of the measured deuteron polarization. The EST predictions for the lithium polarizations, based on the measured deuteron polarization, are shown by the full lines and are in agreement with the data.



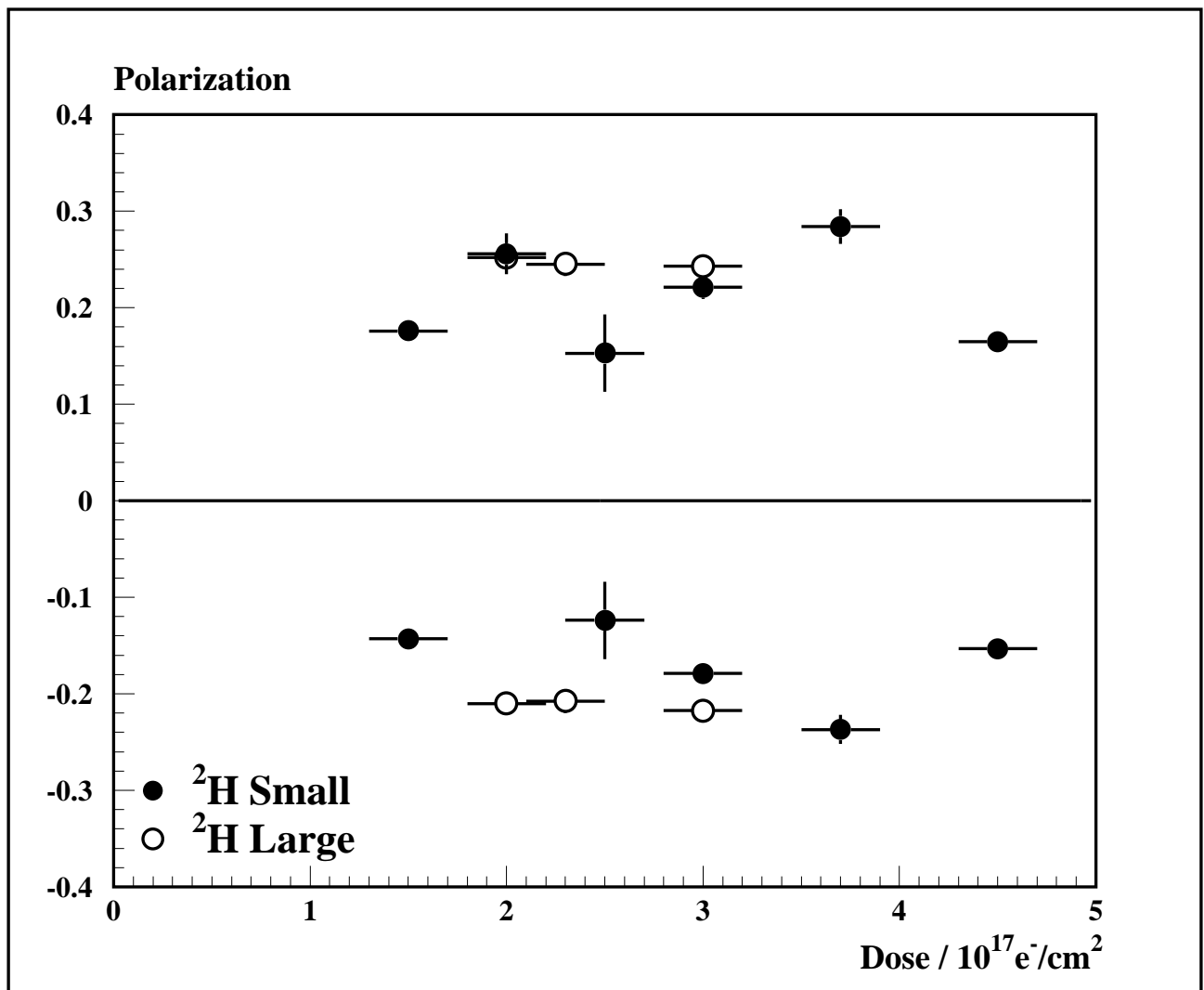


Figure 5: Deuteron polarizations in preirradiated  $^6\text{LiD}$  for different sample sizes and irradiation doses (prior to usage in E155). The deviation of the sample with the  $2.5 \cdot 10^{17} \text{ e}^-/\text{cm}^2$  dose was not understood and might have been due to under-irradiation.

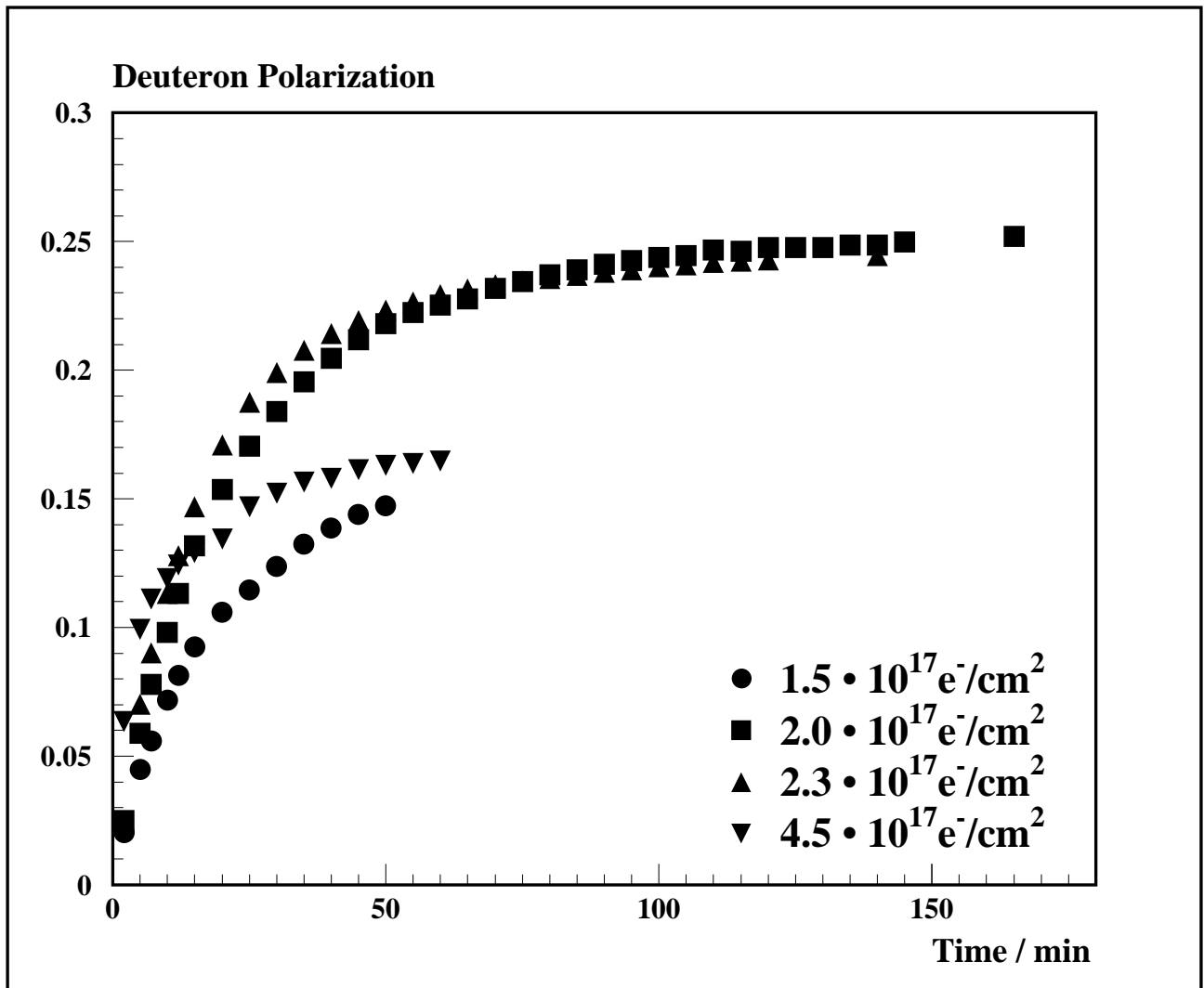


Figure 6: Deuteron polarization build-up of target materials with different pre-irradiation doses.

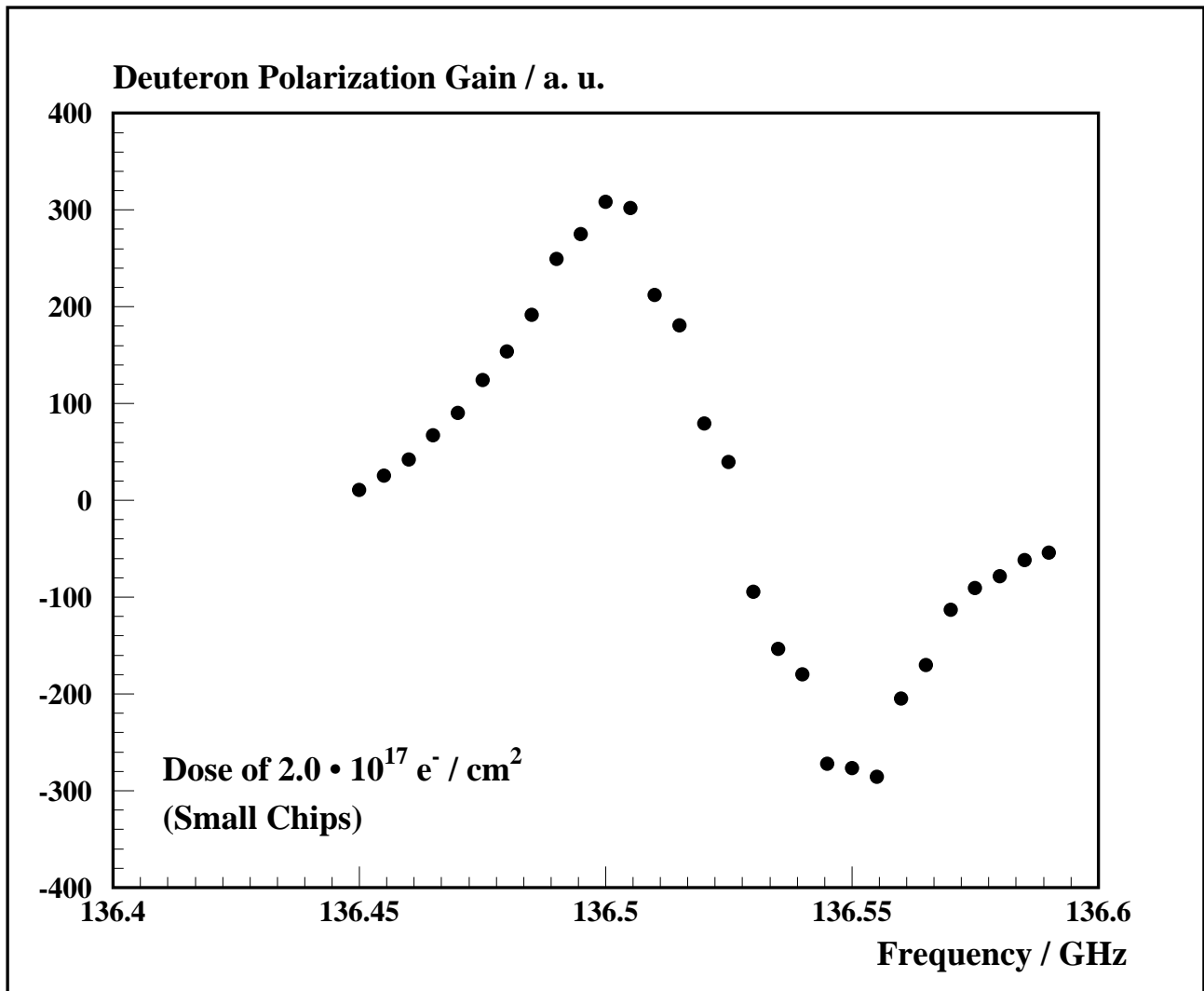


Figure 7: Deuteron polarization gain as a function of the microwave frequency, at a fixed magnetic field of 4.87 T. The separation of about 50 MHz between the optimum polarizing frequencies is typical.

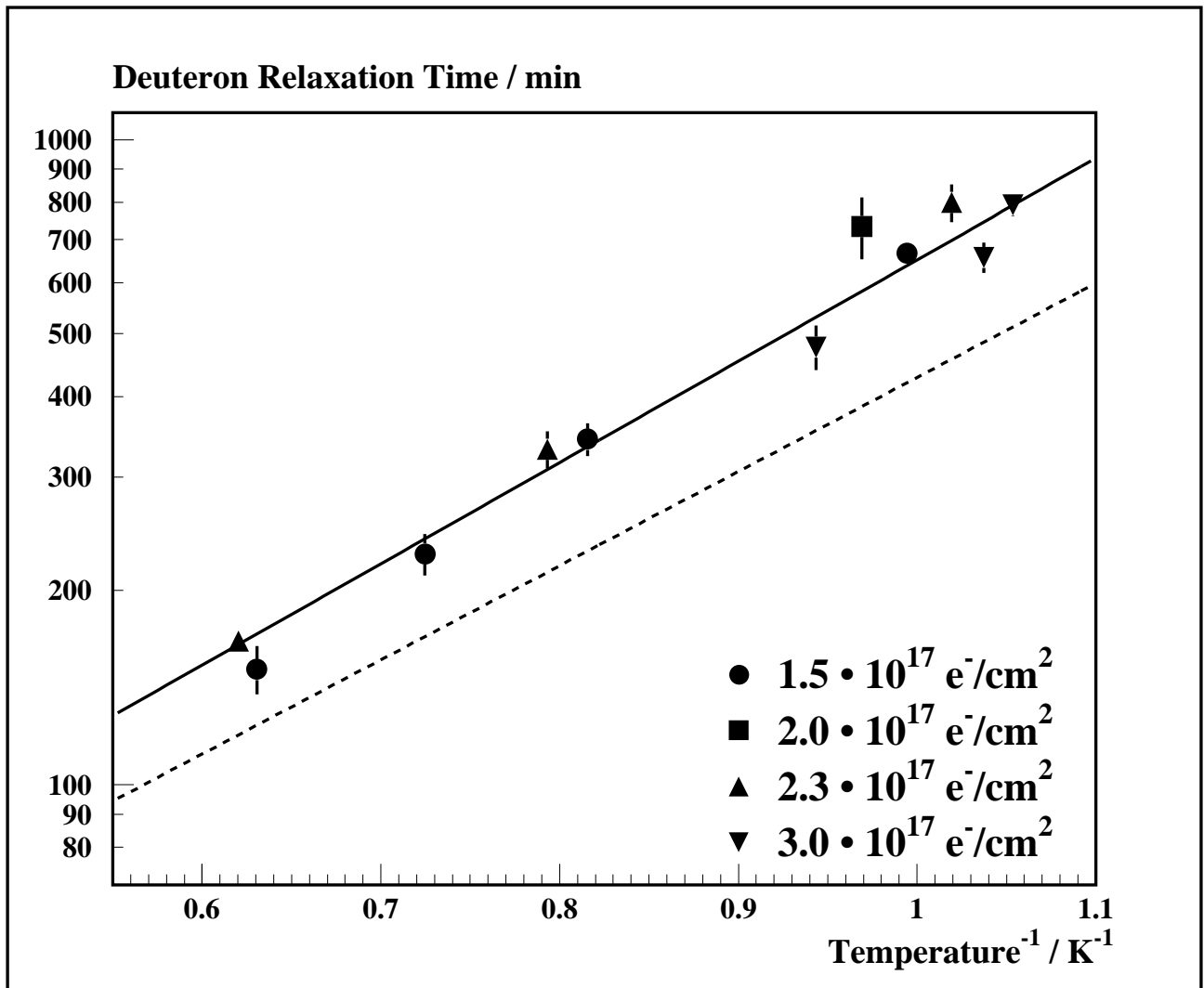


Figure 8: Deuteron relaxation times,  $\tau$ , as a function of  $T^{-1}$  for different pre-irradiation doses. The fit to the data points (full line) results in a  $g$ -factor of  $2.15 \pm 0.17$ , while the slope of the dashed line corresponds to a  $g$ -factor of 2.

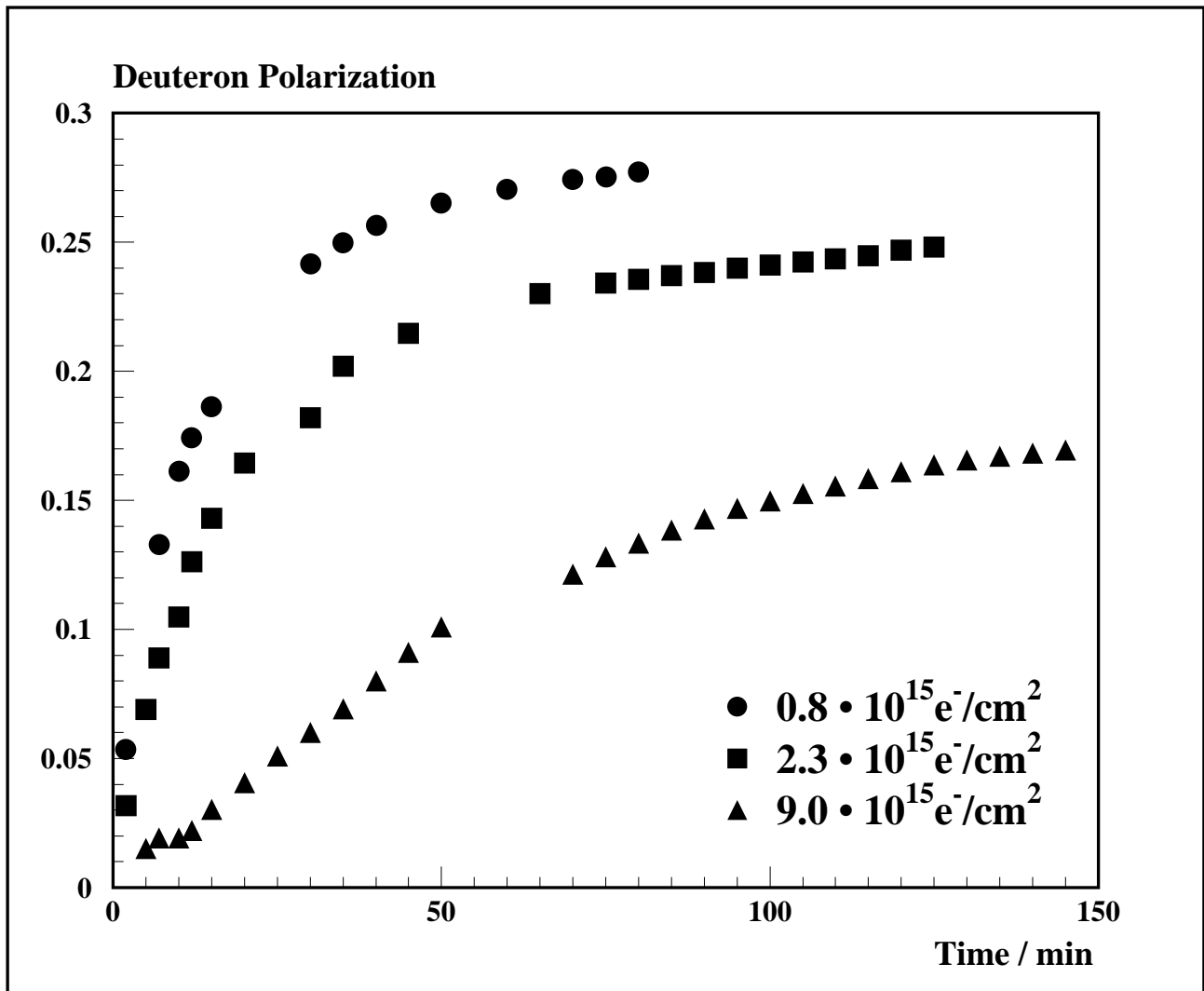


Figure 9: Deuteron polarization build-up of target material with a pre-irradiation dose of  $3.7 \cdot 10^{17} \text{ e}^-/\text{cm}^2$  for three accumulated irradiation doses in the 48 GeV electron beam.

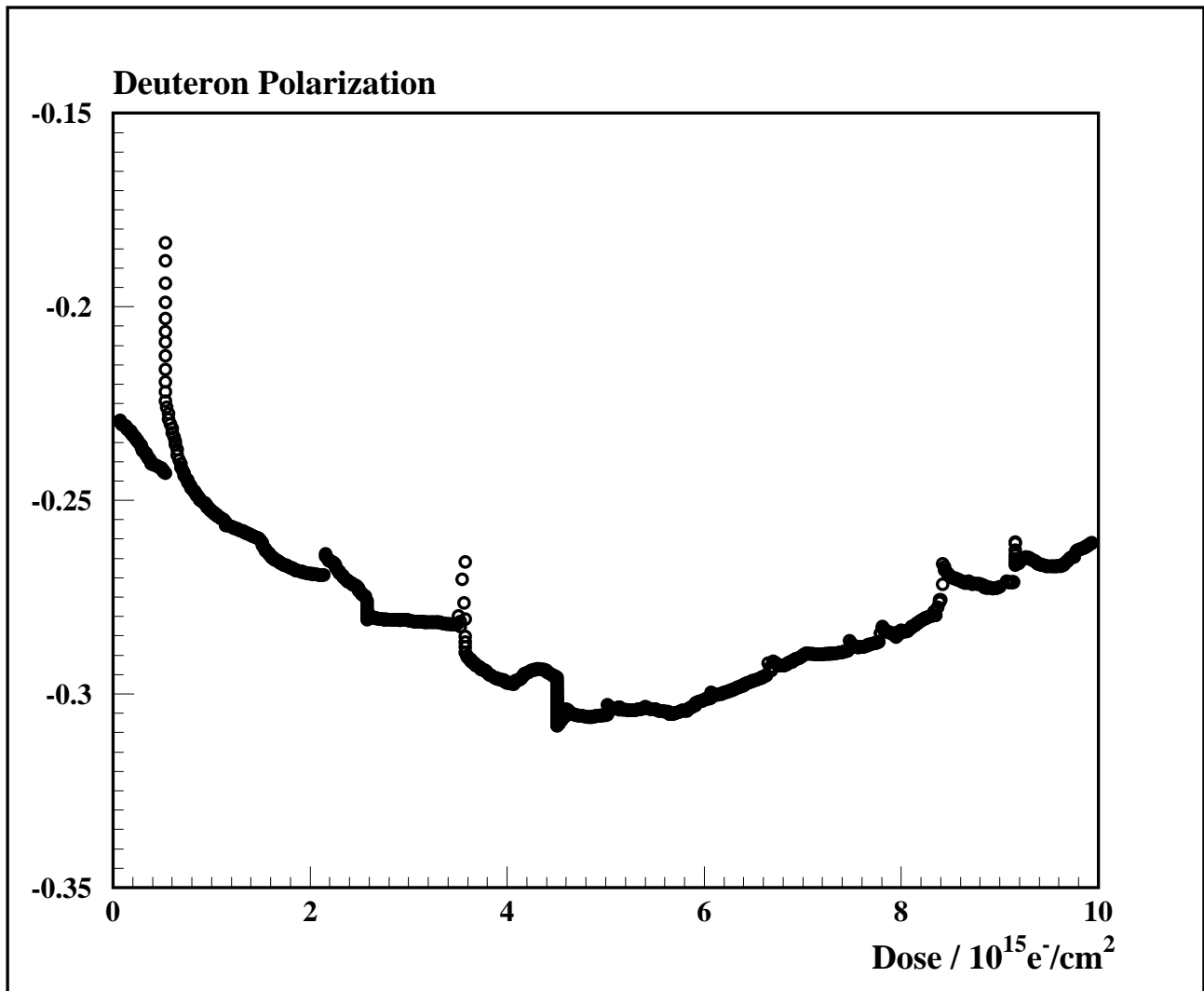


Figure 10: Deuteron polarization of the  $2.0 \cdot 10^{17} \text{ e}^-/\text{cm}^2$  sample as a function of the accumulated dose in the 48 GeV electron beam. Deuterated ammonia shows the same behavior, but with a maximum polarization at about  $10^{15} \text{ e}^-/\text{cm}^2$  [5].